First-principles study of the local structure and crystal field of Yb^{2+} in sodium and potassium halides*

Wen Jun(闻 军)[a], Duan Chang-Kui(段昌奎)[a)†], Yin Min(尹 民)[a)],
Yu. V. Orlovskii[b)c)], Xia Shang-Da(夏上达)[a)], and Zhang Yong-Fan(章永凡)[d)]

[a)] *Department of Physics, University of Science and Technology of China, Hefei* 230026, *China*
[b)] *Prokhorov General Physics Institute RAS, 38 Vavilov st., Moscow* 119991, *Russia*
[c)] *Institute of Physics, University of Tartu, Riia 142, Tartu* 51014, *Estonia*
[d)] *Department of Chemistry, Fuzhou University, Fuzhou* 350002, *China*

(Received 26 October 2011; revised manuscript received 10 November 2011)

The local coordination structures around the doping Yb^{2+} ions in sodium and potassium halides were calculated by using the first-principles supercell model. Both the cases with and without the charge compensation vacancy in the local environment of the doping Yb^{2+} were calculated to study the effect of the doping on the local coordination structures of Yb^{2+}. Using the calculated local structures, we obtained the crystal-field parameters for the Yb^{2+} ions doped in sodium and potassium halides by a method based on the combination of the quantum-chemical calculations and the effective Hamiltonian method. The calculated crystal-field parameters were analyzed and compared with the fitted results.

Keywords: sodium and potassium halides, local coordination structure, distortion, crystal-field parameters

PACS: 71.15.Mb, 71.20.Eh, 78.20.–e, 78.20.Bh **DOI:** 10.1088/1674-1056/21/3/037102

1. Introduction

Lanthanide-ion doped luminescent materials have attracted much attention for decades due to their wide applications in fluorescence lighting, displays, and scintillator detectors.[1−3] The optical properties of luminescent materials depend not only on the lanthanide ion as the dopant, but also strongly on the host.[4] Usually the local structural information provides an important guide for understanding the experimental results and helps in the design of luminescent materials.[5−7] For example, the distortion in the local environment of the doping lanthanide ion may allow certain emission transitions,[8] and also may split or shift the absorption and the emission bands.

Although there are large numbers of experimental studies to explore their structural and luminescence properties,[1−9] the local coordination structures around the doping lanthanide ions cannot be obtained by direct experimental measurements. The first-principles calculations can provide structural information about the doped systems.[10−14]

The energy levels and the transition intensities of lanthanide ions in crystals can be effectively simulated with a crystal-field (CF) Hamiltonian and the electric dipole operator, which involves many parameters relied on fitting to experimental spectroscopic data. Reid *et al.*[15−18] put forward a method to obtain the CF parameters by making use of the energies and the wavefunctions of the first-principles calculations. This method does not rely on the prior experimental spectroscopic data but requires the detailed local structure of the lanthanide ion in the host.

The Yb^{2+}-doped MX series (M = Na and K; X = F, Cl, Br, and I) are chosen as the model systems in this study, since the hosts are of very high symmetry with well known structures, and the CF energy levels and the transitions of Yb^{2+} are sensitive to the local structure and well-characterized.[19−21] There is an M^+ (M = Na and K) vacancy for charge compensation, which may be near or far away from the dopant, and the asymmetry in the environment of the Yb^{2+} ion may have some effect on the optical

*Project supported by the National Natural Science Foundation of China (Grant Nos. 11074315, 11074245, 90922022, and 11111120060), the Russian Foundation for Basic Research (Grant No. 11-02-91152), and the European Social Fund (Grant No. MTT50).

†Corresponding author. E-mail: ckduan@ustc.edu.cn

© 2012 Chinese Physical Society and IOP Publishing Ltd

transitions.[19,20] We firstly study the local coordination structures around the doping ions for the Yb^{2+}-doped MX series (M = Na and K; X = F, Cl, Br and I) by performing the calculations using the supercell model, and then calculate the CF parameters for these systems and compare the parameters with the ones obtained by least-square fitting to the experimental data.[21] We also discuss the effect of the local-structure distortion on the CF and the emission properties of the Yb^{2+}-doped MX series.

2. Computational details

The relaxations of the lattices for MX and the Yb^{2+}-doped MX series have been performed by using the Vienna *ab initio* simulation package (VASP) program.[22−23] The $3s^1$ electron on Na, the $3p^64s^1$ electrons on K, the $2s^22p^5$ electrons on F, the $3s^23p^5$ electrons on Cl, the $4s^24p^5$ electrons on Br, the $5s^25p^5$ electrons on I, and the $5p^66s^2$ electrons on Yb were treated as the valence electrons, and their interactions with the cores were described by the projected augmented wave (PAW) method.[24] The GGA-PW91 exchange–correlation functional has been employed. The ion relaxation was performed using the conjugate gradient technique. Besides, the stopping criterion in energy change per step for the ionic motion was set to be 10^{-4} eV, and the forces acting on the atoms for the relaxation of the atomic positions were checked to be less than 10^{-3} eV/Å. The integration within the Brillouin zone was performed with a Γ-point centered grid of k points. The number of the irreducible k points was chosen to be three for the supercell, and eight for the unit cell. Other parameters of the relaxation studies were set at the standard values of the program.

Firstly, the structural optimization was carried out for the pure MX lattices by starting with the measured lattice parameters. Then the Yb^{2+}-doped MX was modeled by a 2×2×2 supercell containing 64 (or 63 for the case with a charge compensation vacancy) atoms, in which the center M atom was substituted by an Yb atom. Due to the difference between Yb^{2+} and M^+ in charge, the effect of the charge compensation should be taken into account. We considered the following two cases: the 2×2×2 supercell with +1 in total charge for the case when the compensation charge vacancy was far away from Yb^{2+} (case 1); and the 2×2×2 supercell with 0 in total charge for the case with a charge compensation vacancy at the nearest cation site around Yb^{2+} (case 2). For both cases, the atomic coordinates and the lattice parameters were fully relaxed without any constraint on symmetry.

Based on the optimized local coordination structures around the Yb^{2+} ions, the clusters $(YbM_{12}X_6)^{8+}$ (case 1) and $(YbM_{11}X_6)^{7+}$ (case 2) embedded in the microcrystals (containing about 1500 host ions) of the MX host lattices were chosen to perform the quantum-chemical self-consistent relativistic DV-X_α calculations.[25,26] The CF parameters for 4f and 5d orbitals were then calculated from the DV-X_α energies and the wavefunctions by using the effective Hamiltonian method developed by Reid *et al.*[15−17] The following is a brief description of this method.

The molecular orbitals, i.e., the eigenfunctions of the one-electron DV-X_α Hamiltonian, contain not only the center-ion atomic orbitals, such as 4f and 5d orbitals of Ln^{3+} here, but also the atomic orbitals for ligands. All the fourteen 4f (ten 5d) base functions are used to form the 4f (5d) model space. According to the quantum-chemical calculations, the matrices for both the fourteen (ten) eigenvalues with the largest 4f (5d) components and the corresponding eigenvectors projected into the model space are chosen to construct $H_{\rm eff}$ for the 4f (5d) model space. This $H_{\rm eff}$ is then expanded in terms of a complete set of parameters and operators describing the effective interactions in the 4f (5d) model space. Consequently, the 4f (5d) CF parameters are extracted in a straightforward way.

3. Results and discussion

The calculated lattice parameters of the pure MX crystals are listed in Table 1 together with the experimentally measured lattice parameters. It shows that the calculated lattice parameters are in good agreement with the measured ones. This serves as a check of the accuracy of the structural optimization. In Table 2, we summarize the calculated Yb^{2+}–X^- bond lengths for the Yb^{2+}-doped MX series in case 1, and compare them with the calculated M^+–X^- bond lengths and the sums of the Shannon ion radii[33] of M^+ (Yb^{2+}) and X^-. From the relaxation result in case 1, we find that the doping does not cause any distortion to the local coordination structure, and the site symmetry of the Yb^{2+} ion remains O_h. However, the Yb^{2+}–X^- bond lengths are short compared with the M^+–X^- bond lengths. In the NaX:Yb^{2+} series, the calculated Yb^{2+}–X^- bond lengths are just slightly smaller than both the calculated Na^+–X^- bond lengths and the sums of the ion radii of Yb^{2+} and

X^-. However in the KX: Yb^{2+} series, the calculated Yb^{2+}–X^- bond lengths are much smaller than both the calculated K^+–X^- bond lengths and the sums of the ion radii of K^+ and X^- as a result of the bigger difference in the ion radius between Yb^{2+} and K^+. The Yb^{2+}–X^- bond lengths are still very close to the sums of the ion radii of Yb^{2+} and X^- as expected. In case 1, the 2×2×2 supercells chosen to simulate the situation with the charge compensation vacancy far away from the doping Yb^{2+} are not neutral (+1 in total charge). This might make the obtained geometries deviate from the real ones. To examine the influence of the net charge on the optimized result in case 1, we consider the case (case 3) of the 2×2×2 Yb^{2+}-containing NaCl supercell with a Na^+ vacancy at the farthest site from Yb^{2+}. Two optimizations, one with and the other without the restriction of symmetry, are carried out. The optimized bond lengths are listed in Table 3 and compared with those in case 1. It can be seen that the deviation of the optimized Yb^{2+}–Cl^- bond length from that of case 1 is less than 0.3%, much less than the typical systematic error of 1–3% for the DFT-PW91 method adopted. In order to keep the structural symmetries of the supercells, we still adopt the optimized results of case 1 for the MX:Yb^{2+} series to simulate the situation where the vacancy is far away from Yb^{2+}.

Table 1. Calculated and the corresponding measured lattice parameters for MX. Units are angstrom (Å).

Lattice parameters	Measured[27−32]	Calculated
NaCl	5.640	5.673
NaBr	5.974	6.015
NaI	6.479	6.515
KF	5.367	5.467
KCl	6.299	6.413
KBr	6.585	6.731
KI	7.030	7.206

Table 2. Bond lengths and sums of ion radii for various MX:Yb^{2+} without surrounding charge compensation vacancy (case 1), where R_{M^+}, R_{X^-}, and $R_{Yb^{2+}}$ are the Shannon ion radii of M^+, X^-, and Yb^{2+}, respectively, R_{Na^+} = 1.020 Å, R_{K^+} = 1.380 Å, $R_{Yb^{2+}}$ = 1.020 Å, R_{F^-} = 1.330 Å, R_{Cl^-} = 1.810 Å, R_{Br^-} = 1.960 Å, R_{I^-} = 2.200 Å are used in the table. Units are angstrom (Å).

MX	M^+–X^-	Yb^{2+}–X^-	$R_{M^+}+R_{X^-}$	$R_{Yb^{2+}}+R_{X^-}$
NaCl	2.837	2.717	2.830	2.830
NaBr	3.007	2.885	2.980	2.980
NaI	3.258	3.126	3.220	3.220
KF	2.734	2.282	2.710	2.350
KCl	3.207	2.781	3.190	2.830
KBr	3.366	2.946	3.340	2.980
KI	3.603	3.187	3.580	3.220

Table 3. Calculated bond lengths for case 3 of the 2×2×2 Yb^{2+}-containing NaCl supercell with a Na^+ vacancy at the farthest site from Yb^{2+}. Units are angstrom (Å).

Bond length	Case 1	Case 3	
		With constriction of symmetry	Without constriction of symmetry
Yb^{2+}–Cl^-	2.717	2.725	2.725
Yb^{2+}–Na^+	4.050	4.112	4.112

In case 1, we are mainly concerned with the changes of the cation–anion bond lengths induced by the doping. According to Ref. [20], the reported luminescence spectrum of NaCl: Yb^{2+} is composed of two emission bands, the lower-energy emission band (denoted as II, with a peak at 432 nm) has a steady low temperature decay rate of $\sim 700\ s^{-1}$. Theoretically, the emission band II is related to the spin-triplet initial states of the E_u and the T_{2u} levels of the Yb^{2+} ion, whose electric-dipole transitions to the spin-singlet ground state are forbidden by the selection rules of spin and O_h symmetry. The experimental result indicates that there may be distortion in the local environment of the doping Yb^{2+} ion. Consequently, for the Yb^{2+}-doped MX system, there may be a charge compensation vacancy in the local environment of the Yb^{2+} ion. When the vacancy locates at a cation site far away from the dopant site, its effect on the doping ion is weak. A qualitative consideration[21] indicates that the total energy of the system favors a vacancy at the nearest cation site of the dopant site. So we consider case 2, where the charge compensation vacancy is put at the nearest cation site of the doping Yb^{2+} ion.

The calculated local coordination structure around the doping Yb^{2+} ion in NaCl: Yb^{2+} of case 2 is presented in Table 4 and also illustrated in Fig. 1. With a compensation vacancy at the nearest cation

site, the local site symmetry of the doping Yb^{2+} is reduced from O_h to C_{2v}, in which the C_2 axis passes through the Yb^{2+} site and Na11, as shown in Fig. 1. Here we analyze the case of NaCl: Yb^{2+} in detail. In general, the Na^+ vacancy distorts the local coordination structure around the doping Yb^{2+} ion. The calculated Yb^{2+}–Cl^- bond lengths fall into three types of length values, 2.696 Å, 2.739 Å, and 2.754 Å respectively. The calculated Yb–Cl1 and Yb–Cl2 bond lengths (2.696 Å) are shorter than the calculated Yb^{2+}–Cl^- bond length in case 1 (2.717 Å), while the Yb–Cl3 and the Yb–Cl4 bond lengths (2.739 Å) as well as the Yb–Cl5 and the Yb–Cl6 (2.754 Å) bond lengths are longer. In addition, the calculated Cl–Yb–Cl bond angles are not 90° anymore. For example, the calculated bond angle Cl1–Yb–Cl2 widens to 96.3°, while Cl5–Yb–Cl6 narrows to 87.2°. Both bond angles Cl1–Yb–Cl5 and Cl2–Yb–Cl6 narrow to 88.3°. According to the calculated local coordination structure, we can see that all the six nearest Cl^- ions around the doping Yb^{2+} ion tend to stay away from the Na^+ vacancy. This is conceivable, as there is a lack of the Coulomb attraction from the missing Na^+ ion for the nearest Cl^- ions. From another point of view, it can be seen that if the local coordination ions are approximately fixed, the Yb^{2+} ion then tends to move slightly towards the Na^+ vacancy. The barycenter of the six nearest Cl^- ions is at the location (−0.060, −0.060, 0) when Yb^{2+} is set as the origin of the coordinative system. This means that Yb^{2+} shifts diagonally on the xy plane to (0.060, 0.060, 0) with respect to the barycenter of the six surrounding Cl^- ions. The distortions appeared in the other Yb^{2+}-doped MX crystals are similar to that in the case of NaCl: Yb^{2+}. This important information on the local coordination structures cannot be obtained directly from the experimental results, although they are useful for the calculations of CF energy level splittings, 4f–5d electric dipole strength, and electron paramagnetic resonance of the Yb^{2+} ions in the MX: Yb^{2+} series.

Table 4. Calculated local coordination structure of NaCl: Yb^{2+} with a charge compensation vacancy at one of the nearest Na^+ sites (case 2), where x, y, and z are the ion coordinates, d is the Yb–Cl bond length. Units are angstrom (Å).

Atom	x	y	z	d
Yb	0.000	0.000	0.000	0.000
Cl1	–0.147	2.692	0.000	2.696
Cl2	2.692	–0.147	0.000	2.696
Cl3	–0.044	–0.044	2.738	2.739
Cl4	–0.044	–0.044	–2.738	2.739
Cl5	–2.753	–0.067	0.000	2.754
Cl6	–0.067	–2.753	0.000	2.754

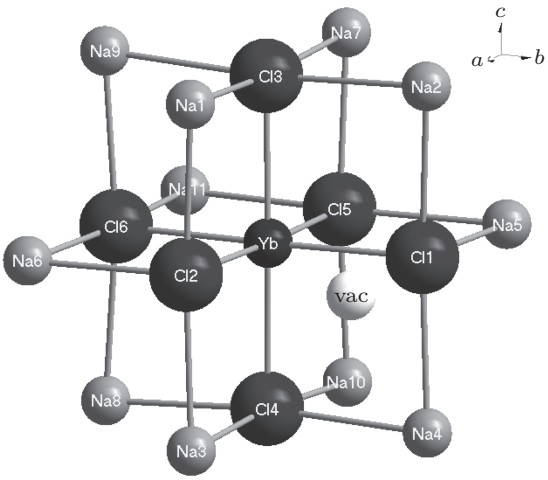


Fig. 1. Calculated local coordination structure around the doping Yb^{2+} ion in NaCl: Yb^{2+} with a charge compensation vacancy at one of the nearest Na^+ sites (case 2). The white ball labeled vac represents the Na^+ vacancy.

Once the calculated local coordination structures around the Yb^{2+} ions in MX: Yb^{2+} are obtained, the CF parameters for the Yb^{2+} ions doped in the MX crystals can be derived by the method mentioned above. In this work, we are interested in the CF parameters of the 5d orbitals. For the Yb^{2+}-doped MX series in case 1, the calculated 5d CF parameters B_0^4 are shown in Fig. 2, compared with the fitted results reported in Ref. [21]. In case 1, the Yb^{2+} ions occupy the sites of O_h symmetry. The nonzero 5d CF parameters are B_0^4 and B_4^4. Note that for the O_h symmetry, the ratio of B_4^4 to B_0^4 is fixed, i.e., $\eta = B_4^4/B_0^4 = \sqrt{5/14}$. So we only give the B_0^4 values. It can be seen that B_0^4 decreases across the Yb^{2+}-doped sodium (potassium) halide series. Besides, for the same halogen element, B_0^4 of the Yb^{2+}-doped sodium halide is larger than that of the Yb^{2+}-doped potassium halide. The trend of the decrease of the CF parameter with respect to the increase of the Yb^{2+}–X^- bond length is illustrated in Fig. 2. Our calculated results are qualitatively in good agreement with the fitted results, in consideration of the precision of the DV-X_α calculations.

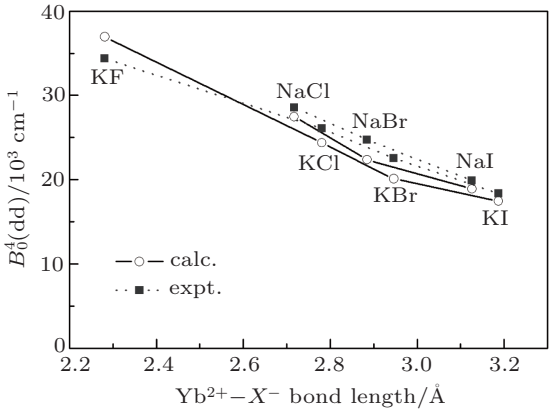


Fig. 2. Calculated CF parameter B_0^4 of the Yb^{2+}-doped MX series without surrounding charge compensation vacancy (case 1), compared with the ones obtained by least-square fitting to the experimental data in Ref. [21].

In case 2, as the charge compensation vacancy is near Yb^{2+}, the local site symmetry of the doping Yb^{2+} ion is reduced to C_{2v}. The nonzero 5d CF parameters are B_0^2, B_2^2, B_0^4, B_2^4, and B_4^4. All the calculated 5d CF parameters of the Yb^{2+} ions doped in the MX series are listed in Table 5. It can be seen that although the compensation vacancy and the local structural distortion exist in the environment of the doping Yb^{2+} ion in case 2, the main parts of the CF parameters, i.e., B_4^4 and B_0^4, change only slightly compared with those in case 1. The ratios (η) of B_4^4 to B_0^4 for the Yb^{2+} sites in the Yb^{2+}-doped MX series are also listed in Table 5. The ratios show that the deviation of the CF parameters from those of the O_h cases is small. Besides B_0^4 and B_4^4, other parameters B_0^2, B_2^2, and B_2^4 are also obtained, which turn up due to the deviation from the O_h site symmetry and as the result of the vacancy and the distortion. The values of these low-symmetry parameters agree qualitatively with those reported in Ref. [21] for the case including the vacancy but not the distortion due to the introduction of the vancancy. The reduction of the site symmetry of the doping Yb^{2+} ion induced by the small distortion has a small but nontrivial effect to the emission of the Yb^{2+}-doped MX series, i.e., it induces the splittings of the CF energy levels (such as E_u and T_{2u} energy levels mentioned previously) and the mixing among the states. Consequently, the transitions from the low-energy excited states of $4f^{13}5d$ become partially allowed, although they are forbidden under the O_h symmetry approximation.

Table 5. Calculated 5d CF parameters for the Yb^{2+}-doped MX series with a charge compensation vacancy at one of the nearest Na^+ sites (case 2). For O_h symmetry, $\eta = B_4^4/B_0^4 = 0.598$. Units are cm^{-1}.

Parameters	NaCl	NaBr	NaI	KF	KCl	KBr	KI
B_0^2	–481	–387	–247	–819	–572	–500	–470
B_2^2	–568	–12	120	359	–253	–121	88
B_0^4	26375	21744	18661	37668	23802	19980	16208
B_2^4	952	–15	–140	–674	241	–16	–339
B_4^4	15415	12863	10704	20847	14725	12100	9611
η	0.585	0.592	0.574	0.553	0.619	0.606	0.593

4. Conclusion

In summary, we have calculated the local coordination structures and the CF parameters of the Yb^{2+} doped in the MX (M = Na and K; X = F, Cl, Br, and I) crystals. The results show that 1) for the case without a nearest cation charge-compensation vacancy, the doping causes a contraction of the Yb^{2+}–X^- bond lengths with respective to the M^+–X^- bond lengths; 2) for the case of charge compensation with a vacancy at the cation site nearest to Yb^{2+}, there is a clear local coordination structure distortion, which has been given explicitly; 3) the trend of the variation of the CF parameters calculated for the Yb^{2+}-doped MX series is in good agreement with those values determined by fitting to the measured levels. The method presented in this paper can be used to predict the effect of the local structural distortion on the CF splitting and the 4f–5d transitions of the doping lanthanide ions.

References

[1] Mao J G 2007 *Coord. Chem. Rev.* **251** 1493
[2] Bünzli J C G 2010 *Chem. Rev.* **110** 2729
[3] Wei X D, Cai L Y, Lu F C, Chen X L, Chen X Y and Liu Q L 2009 *Chin. Phys.* B **18** 3555
[4] Xie R J and Hirosaki N 2007 *Sci. Technol. Adv. Mater.* **8** 588
[5] Shen Y R and Bray K L 1998 *Phys. Rev.* B **58** 11944
[6] Wang F, Han Y, Lim C S, Lu Y H, Wang J, Xu J, Chen H Y, Zhang C, Hong M H and Liu X G 2010 *Nature* **463** 1061

[7] Canning A, Chaudhry A, Boutchko R and Jensen N G 2011 *Phys. Rev.* B **83** 125115

[8] Duan C K, Tanner P A, Meijerink A and Makhov V 2011 *J. Phys. Chem.* A **115** 9188

[9] Wei X T, Zhao J B, Chen Y H, Yin M and Li Y 2010 *Chin. Phys.* B **19** 077804

[10] Dorado B, Jomard G, Freyss M and Bertolus M 2010 *Phys. Rev.* B **82** 035114

[11] Singh D J 2010 *Phys. Rev.* B **82** 155145

[12] Andriessen J, van der Kolk E and Dorenbos P 2007 *Phys. Rev.* B **76** 075124

[13] Stephan M, Zachau M, Gröting M, Karplak O, Eyert V, Mishra K C and Schmidt P C 2005 *J. Lumin.* **114** 255

[14] Chen Z L, Zou H M, Zhu X P, Zou J and Cao J F 2011 *J. Solid State Chem.* **184** 1784

[15] Reid M F, Duan C K and Zhou H W 2009 *J. Alloys Compd.* **488** 591

[16] Reid M F, Hu L S, Frank S, Duan C K, Xia S D and Yin M 2010 *Eur. J. Inorg. Chem.* **18** 2649

[17] Hu L S, Reid M F, Duan C K, Xia S D and Yin M 2011 *J. Phys.*: *Condens. Matter* **23** 045501

[18] Hu L S, Wen J, Xia S D and Yin M 2010 *J. Rare Earth.* **28** 899

[19] Tsuboi T, Witzke H and McClure D S 1981 *J. Lumin.* **24–25** 305

[20] Tsuboi T, McClure D S and Wong W C 1993 *Phys. Rev.* B **48** 62

[21] Duan C K and Tanner P A 2008 *J. Phys.*: *Condens. Matter* **20** 215228

[22] Kresse G and Furthmüller J 1996 *Phys. Rev.* B **54** 11169

[23] Kresse G and Joubert D 1999 *Phys. Rev.* B **59** 1758

[24] Blöchl P E 1994 *Phys. Rev.* B **50** 17953

[25] Rosen A and Ellis D E 1975 *J. Chem. Phys.* **62** 3039

[26] Adachi H, Tsukada M and Satoko C 1978 *J. Phys. Soc. Japan* **45** 875

[27] Nickels J E, Fineman M A and Wallance W E 1949 *J. Phys. Chem.* **53** 625

[28] Davey W P 1923 *Phys. Rev.* **21** 143

[29] Finch G J and Fordham S 1936 *Pro. Phys. Soc. London* **48** 85

[30] Walker D, Verma P K, Cranswick L M D, Jones R L, Clark S M and Buhre S 2004 *Am. Mineral.* **89** 204

[31] Ahtee M 1969 *Ann. Acad. Sci. Fenn. Series A6: Phys.* **311** 1

[32] Cortona P 1992 *Phys. Rev.* B **46** 2008

[33] Shannon R D 1976 *Acta Cryst.* A **32** 751